This is the accepted manuscript of: Rostán, S., Laing, S., Girard, A., Scalese, G., Cooper, A., MacLeod, A., Pérez-Díaz, L., Mahler, G., Faulds, K., Graham, D., & Otero, L. (2024). Gold nanoparticle-based conjugated nanotags as potential compounds against Trypanosoma brucei infection. *ACS Applied Nano Materials*, *7*(24), 28219-28228. https://doi.org/10.1021/acsanm.4c05201.

Gold Nanoparticle-Based Conjugated Nanotags as Potential Compounds Against *Trypanosoma brucei* Infection

Santiago Rostán[1,2], Stacey Laing[3], Alexandre Girard[3,4], Gonzalo Scalese[1], Anneli Cooper[4], Annette MacLeod[4], Leticia Pérez-Díaz[5], Graciela Mahler[6], Karen Faulds[3], Duncan Graham[3] and Lucía Otero[1*]

[1] Área Química Inorgánica, Departamento Estrella Campos, Facultad de Química, Universidad de la República, Montevideo, 11800, Uruguay

[2] Graduate Program in Chemistry, Facultad de Química, Universidad de la República, Montevideo, 11800, Uruguay.

[3] Department of Pure and Applied Chemistry, Technology and Innovation Centre, University of Strathclyde, 99 George Street, Glasgow, G1 1RD, U.K.

[4] School of Biodiversity, One Health and Veterinary Medicine, College of Medical, Veterinary and Life Sciences, University of Glasgow, Glasgow, G61 1QH, United Kingdom.

[5] Sección Genómica Funcional, Instituto de Química Biológica, Facultad de Ciencias, Universidad de la República, Montevideo, 11400, Uruguay.

[6] Laboratorio de Química Farmacéutica, Departamento de Química Orgánica, Facultad de Química, Universidad de la República, Montevideo, 11800, Uruguay.

Abstract

In the search for alternatives for the treatment of parasitic Neglected Tropical Diseases (NTD), an approach combining metal-based drug design and nanotechnology has been developed. On one hand, a potential metal-based drug of the formula [PdCl(L1)], where L1 is a coumarin-thiosemicarbazone hybrid ligand, had been previously reported. This compound demonstrated activity *in vitro* and *in vivo* against *Trypanosoma cruzi*, the etiological agent of Chagas disease. On the other hand, conjugation of gold nanoparticles

This is the accepted manuscript of: Rostán, S., Laing, S., Girard, A., Scalese, G., Cooper, A., MacLeod, A., Pérez-Díaz, L., Mahler, G., Faulds, K., Graham, D., & Otero, L. (2024). Gold nanoparticle-based conjugated nanotags as potential compounds against Trypanosoma brucei infection. *ACS Applied Nano Materials*, *7*(24), 28219-28228. https://doi.org/10.1021/acsanm.4c05201.

(AuNPs) to biologically active compounds has shown to enhance drug delivery and efficacy. In this work, these approaches were combined to successfully conjugate [PdCl(L1)] with AuNPs containing a Raman reporter for intracellular tracking. The aim of this conjugation was to exploit the potential of the nanoparticles as carriers and of the metal complex as an antiparasitic agent. Conjugated nanotags were fully characterized and both the free palladium complex and the conjugates were tested against *Trypanosoma brucei brucei* (*T.b.b*), the causative agent of a related NTD, African Trypanosomiasis. The results showed that the conjugated nanotags [Pd(L1)-AuNPs] (IC_{50} = 3.22 μM) demonstrated almost a fivefold increase in the anti-*T.b.b*. activity in comparison with [PdCl(L1)] alone (IC_{50} = 15.32 μM) and twice the activity of the unconjugated nanoparticles (IC_{50} = 6.14 μM). In addition, the preliminary imaging using Raman microscopy and surface enhanced Raman scattering (SERS) experiments revealed successful uptake of [Pd(L1)-AuNPs] by parasites. Although the *in vitro* selectivity was not improved post-conjugation, the promising anti-trypanosomatid activity of these conjugates warrant evaluation for performance and selectivity through future *in vivo* studies. This research paves the way for further exploration of the developed strategy in the fight against parasitic infections.

Keywords: gold nanoparticles, metal-based drugs, palladium complex, trypanosomatid parasites, SERS

1. Introduction

Inorganic Medicinal Chemistry (IMC) is a rapidly growing field at the intersection of inorganic chemistry and medicine. It focuses on the development and understanding of metal-based drugs as treatment or diagnostic agents. These drugs, often called metallodrugs, are fundamentally different from traditional organic drugs in their structure and mechanisms of action. A usual approach in IMC is the coordination of a bioactive organic drug to a metal center, leading to new species with different physicochemical and

biological properties. If the metal is also bioactive (can interact somehow with biological entities) as for example Pt(II) or Pd(II) then the resulting compound may have a dual mode of action (one due to the ligand's activity and the other due to the activity of the metal center)[1,2]. This approach has been explored for the development of metal compounds with potential activity against the *Trypanosoma cruzi* (*T. cruzi*) parasite[3,4]. This pathogen is the etiological agent of Chagas Disease (CD) which is endemic in most regions of South America. The World Health Organization (WHO) has catalogued CD as a Neglected Disease since it affects around 7 million people and the efforts and investments to find more effective treatments for the disease are challenging and come mainly from academia rather than industry[5,6].

One of the compounds recently developed by our group, a Pd-coumarin-thiosemicarbazone complex, **[PdCl(L1)]** (Figure 1)**,** has shown a promising anti-parasitic profile, decreasing the amount of trypomastigotes and amastigotes of *T. cruzi in vitro* and lowering parasitaemia in the *in vivo* assays. This compound did not show signs of toxicity in the lactate dehydrogenase (LDH) assay *in vitro* and furthermore, it did not induce death in any of the mice during the *in vivo* assessment[7], thus demonstrating biocompatibility of the compound.

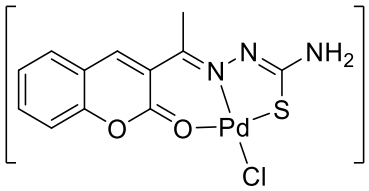

[PdCl(L1)]

Figure 1. Schematic representation of **[PdCl(L1)]**

Related to *Trypanosoma cruzi*, the African trypanosome, *Trypanosoma brucei*, is responsible for Human African trypanosomiasis (HAT), also known as sleeping sickness. This life-threatening disease is caused by two subspecies, *T. b. gambiense* in West and Central Africa, and *T. b. rhodesiense* in East Africa[8]. It is endemic to sub-Saharan Africa and affects mostly poor rural populations. However, travellers to these regions are also at risk. HAT is transmitted through the bite of an infected tsetse fly (*Glossina* spp.). The parasite multiplies in the bloodstream of the host and invades the tissues, and eventually

the central nervous system, where it causes progressive symptoms, including headache, fatigue, sleep cycle disruption, and confusion[9]. If left untreated, HAT can be fatal. A third subspecies, *T.b. brucei*, only infects animals but its ease of handling and genetic similarity to the human-infective subspecies makes it a valuable experimental model for drug discovery. As for CD, the drugs available for the treatment of HAT have many side effects. The therapy depends on the infecting subspecies of the parasite and the stage of the disease being the most used drugs: Pentamidine, Fexinidazole, Nifurtimox, Eflornithine or a combination of them for *T. b. gambiense* and Suramin or Melarsoprol for *T. b. rhodesiense* [10]. For both diseases, the search for new alternatives is also neglected by the industrial sector since these diseases are mostly prevalent in poor rural areas. Many metabolic routes are shared between these trypanosomatid parasites, which could provide a window to create new multispectral drugs[11,12].

In this work, the previously reported **[PdCl(L1)]** complex was tested as an anti *T. brucei* agent against the *T.b. brucei* subspecies. In addition, and to explore new ways of drug delivery for anti-trypanosomatid parasitic compounds, our group have focused on the development of new supramolecular entities. These systems hold promise to enhance targeting potency and uptake within parasitic cells, thereby improving overall efficacy. Gold nanoparticles (AuNPs) are an attractive candidate for this approach with many desirable physicochemical properties for biological applications such as easy synthesis, straightforward surface modification, large surface to volume ratio and size tunability. In addition, they are ideal for drug-delivery because they are nontoxic and nonimmunogenic[13] and as such, have already been employed to deliver anti-cancer platinum based drugs[14,15]. Moreover, AuNPs have been reported to present anti-parasitic and, in particular, anti-trypanosomatid activity in many cases[16–20]. An added benefit of using AuNPs is that they give rise to enhanced Raman scattering of Raman-active molecules (known as Raman reporters) attached to the gold surface. This allows the AuNPs to be imaged using Raman microscopy approaches, which could enable drug tracking[21–23]. Therefore, the **[PdCl(L1)]** complex was linked to functionalized gold nanoparticles containing a Raman reporter, Malachite Green isothiocyanate, (Figure 2) to test whether the anti-parasitic activity was increased upon linkage and to measure the

effect of the AuNPs on non-specific toxicity. The presence of the reporter was desirable to enable monitoring of the nanotags in biological media using Surface Enhanced Raman Scattering (SERS). In this work, imaging experiments of the nanotag treated parasites were also performed in order to monitor the uptake of the drug-nanoparticle conjugates.

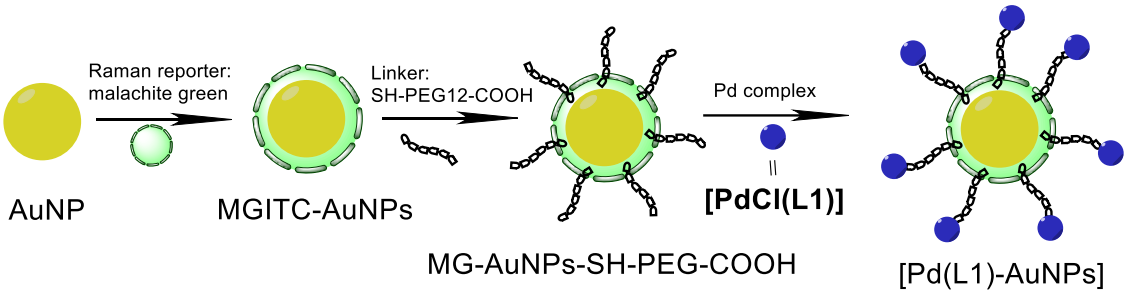

Figure 2. Schematic representation of **[Pd(L1)-AuNPs]** preparation.

2. *Materials and Methods*

2.1. Synthesis and characterization of [PdCl(L1)]

[PdCl(L1)] was prepared and characterized as in the recently reported work by our group[7]. For the synthesis, in brief, a solution of 0.3 mmol of the free neutral coumarin-thiosemicarbazone ligand (Figure 1), HL1 (78 mg) in 10 mL of methanol was added to a suspension of 0.3 mmol of $Na_2[PdCl_4]$ (88 mg) in 10 mL of boiling benzene. The mixture was heated under reflux. After 2 h, an orange microcrystalline solid was isolated by filtration and washed with cold methanol (2×5 mL). Recrystallization from DMF:methanol (1:9 v/v) was carried out as a purification method.

2.2. Synthesis of gold nanotags (MGITC-AuNPs)

Gold nanoparticles (AuNPs) were synthesized using a citrate reduction method previously reported by Turkevich *et al*[24]. More specifically, sodium tetrachloroaurate dihydrate solution (10 mL, 15 mM) was diluted to a final volume of 500 mL in double distilled deionized H_2O ($dddH_2O$) and heated until boiling under continuous stirring. Sodium citrate tribasic dehydrate solution (7.5 mL, 26 mM) was then added and the mixture was boiled under continuous stirring for approximately 1 hour. The resulting

colloidal solution was then left to cool, maintaining stirring throughout. Following this, the AuNPs were functionalized with a selected Raman reporter, Malachite Green isothiocyanate (MGITC), to create simple nanotags (MG-AuNPs). For the functionalization, a final concentration of 40 nM MGITC was used, as it results in a strong SERS signal without inducing aggregation of the colloidal suspension. Briefly, 4 µL of a stock of 10 µM MGITC in water was added to 900 µL of AuNPs, and then dddH_2O was added to a final volume of 1000 µL. Then, the samples were incubated on a shaker plate for 30 minutes and centrifuged at 2348 g for 20 minutes. The resulting pellet was redissolved in 1 mL of dddH_2O. Centrifugation and resuspension steps were repeated twice for each sample in order to purify the obtained nanotags.

2.3. Functionalization of (MGITC-AuNPs) and conjugation to [PdCl(L1)]

To 1 mL of MGITC-AuNPs, a 1 mM stock of carboxy-PEG12-thiol (CTPEG12) was added to a final concentration of 5 µM. The mixture was shaken for 24 hours at room temperature. After this time, 50 µL of borate buffer (0.5 M, pH = 8.5) was added to the mixture and then these nanoparticles were treated with different volumes of a 1.25 mg/mL **[PdCl(L1)]** stock in dimethylformamide (DMF). The samples were shaken again for 24 hours and then centrifuged at 1500 g for 20 minutes. Finally, the pellet was redissolved in 1 mL dddH_2O to obtain a suspension of **[Pd(L1)-PEG-MGITC-AuNPs]** that will be referred to as **[Pd(L1)-AuNPs]** for simplicity. Centrifugation and resuspension steps were repeated twice for each sample in order to remove any unbound molecules from the obtained nanoparticle conjugates.

2.4. Characterization of gold nanotags (MGITC-AuNPs) and [PdCl(L1)] conjugated nanoparticles ([Pd(L1)-AuNPs])

Extinction spectra were measured using an Agilent Cary 60 UV-Visible spectrophotometer with Win UV scan V.2.00 software. Initially the system was left to equilibrate at RT, followed by the insertion of poly(methyl methacrylate) (PMMA) disposable plastic micro cuvettes with 500 µL of sample in order to scan wavelengths from 300 – 800 nm. A baseline was previously obtained using dddH_2O in place of the sample.

A Malvern Zetasizer nano ZS system was used to conduct size and zeta potential measurements. Samples were added to a poly(methyl methacrylate) cuvette with 1 cm path length for all measurements. For zeta potential measurements, a dip cell was placed in the cuvette.

For SERS solution analysis, a Snowy Range CBEx 2.0 handheld Raman spectrometer (Snowy Range Instruments, Laramie WY USA) equipped with a 638 nm laser excitation with a maximum laser power of 40 mV was used. For each measurement, 500 µL of sample was inserted into a glass vial and the SERS spectra were collected using 100% laser power and 1 s accumulation time. For the control measurement, 500 µL of ethanol was inserted into a glass vial and the SERS spectra were collected using the same method. Peak 1.1.112. software was used to acquire the spectra (n = 3 replicates within each condition), which were then baseline corrected in Origin Pro 2018 software.

Size measurements using Scanning Electron Microscopy (SEM) were performed in a FEI Quanta 250 FEGSEM microscope with an electronic beam of 5 kV. The nanoparticle diameter was measured using the software ImageJ® and measuring at least 100 nanoparticles per image.

2.5. Inductively coupled plasma mass spectrometry (ICP-MS) measurements for Pd and Au determination and estimation of Pd load on [Pd(L1)-AuNPs]

An 7700X ICP-MS instrument manufactured by Agilent Technologies (California, USA) was used throughout. The used RF power was 1600W, with a sample depth of 8 mm and using a flow of 3.6 mL/min of the carrier gas (He) and a nebuliser pump speed 0.1 rps.

The Pd load on **[Pd(L1)-AuNPs]** was estimated using the determined quantities of Pd and Au by ICP-MS and also considering ideal spherical nanoparticles in:

$$V_{AuNPs} = 4/3\ \pi\ r_{SEM}^3,$$

where V_{AuNPs} is the calculated volume of the average nanoparticles and r_{SEM} is the average radii of AuNPs determined by SEM measurements. A volume of Au unit cell of 0.0679 cm^3 was used for the estimation[25].

2.6. Parasite cell models

2.6.1 *Trypanosoma brucei* cell culture

Bloodstream form *Trypanosoma brucei brucei*, strain AnTat 1.1E parasites genetically engineered to express a tdTomato red fluorescent protein, were used in this study (gift of B. Rotureau, Institut Pasteur, France)[1]. Axenic parasite cultures were maintained in HMI-9 medium[2] (Life Technologies, ME110145P1) supplemented by 10% heat inactivated Fetal Bovine Serum (Gibco, 10500064) at 37°C with 5% CO_2.

2.6.2 Compound screening assays for *T. b. brucei*

Assays were performed in 96-well flat bottom polystyrene plates (Corning, 3596) containing 193 µL/well of *T. b. brucei* parasites at a starting density of $1x10^5$ cells/mL. An initial screening solution for each compound was added in a volume of 7 µL/well to obtain a final concentration of 25 µM. Controls were added, including HMI-9 culture media only, metal salt $Na_2[PdCl_4]$) and nanoparticles without conjugation (AuNPs and MGITC-AuNPs). Every sample was tested in triplicate. After 24 h incubation at 37°C in 5% CO_2, the number of live trypanosomes were determined by fluorescent cell counting using a Guava® easyCyte 12HT flow cytometer (Millipore Technologies, USA). Cell counts for each compound relative to the *T. b. brucei*-only control were compared by Ordinary One-way ANOVA and Dunnett's multiple comparisons test using GraphPad Prism 10 software.

2.6.3 IC_{50} studies on *T. b. brucei*

Following the initial screening of compounds for anti-trypanosome activity at 25 µM, the *T. b. brucei* assays were repeated across a greater concentration range using a 2-fold dilution series of each compound (50, 25, 12.5, 6.25, 3.12 and 1.06 µM) and diluent-only controls. After 24 h incubation at 37°C in 5% CO_2, the number of live trypanosomes were determined by fluorescent cell counting using a Guava® easyCyte 12HT flow cytometer (Millipore Technologies, USA). IC_{50} values were determined using Non-linear Regression, log(inhibitor) *vs* normalized response model, in GraphPad Prism 10 software.

2.6.4 Slides preparation for Raman Confocal Microscopy

In a 12 well plate, 1 mL containing 1x10^5 *T. b. brucei* parasites in HMI-9 culture media was added to each well. Each sample was prepared in duplicates with a 2 mL volume for fixing steps. 35 µL of the corresponding stock of the selected compounds were added to final concentrations of 2.5 µM and 0.25 µM. The plate was incubated for 5 h at 37°C in 5% CO_2 and then the replicates were combined for each sample into a 15 mL falcon tube (final volume of 2 mL). The samples were centrifuged at 700 g for 7 min, the supernatant was removed and 1 mL 1× PBS was added. The centrifugation – wash process was repeated thrice, and the resulting pellet was treated with 1 mL of 4 % PFA. The samples were then incubated for 15 min at room temperature. Finally, the samples were centrifuged, washed with 1× PBS two more times, and the fixed cell pellets resuspended in 500 µL sterile distilled water. 50 µL of the fixed cell suspension was applied to the glass slides and left to dry.

2.6.5 Raman Confocal Microscopy

A Renishaw InVia Raman confocal microscope equipped with a Leica 20x/NA 0.4 N PLAN EPI objective and a 532 and 633 nm laser excitation source was used. A grating of 1800 l mm^{-1} in high confocality mode and a laser power of 12 mW (100% power) with a 1 s acquisition time per point were used to map gelatin areas. The 2D maps were collected with a spatial resolution of 5 µm in the X and Y directions. The laser resolution was 1.9 µm as calculated for the selected excitation wavelength and microscope objective.

2.7. Mammalian cell models

2.7.1 Compounds´ treatment

The compound **[PdCl(L1)]** was initially dissolved in DMSO at 11.25 mM (stock concentration). The solution was diluted in the culture medium to obtain the different concentrations tested. Throughout the experimental procedures, the concentration of

DMSO never exceeded 1%, which is non-toxic for the cells[26]. **[Pd(L1)-AuNPs]** and **MGITC-AuNPs** were diluted in culture media to obtain the desired concentrations.

2.7.2. VERO cells

VERO cells (ATCC CCL81) were used as a mammalian cell model for testing unspecific cytotoxicity. Cells were cultured in RPMI medium (Gibco) supplemented with 10 % heat inactivated fetal bovine serum, penicillin (100 units/mL) and streptomycin (100 µg/mL) at 37 °C in a humidified 5 % CO_2 incubator. For the cytotoxicity assay, 1000 cells per well were seeded in a 96 well plate in RPMI medium and were incubated at 37 °C in a 5 % CO_2 atmosphere. Once adhered to the plate, cells were incubated with the indicated compound concentrations for 24 h[26–29].

2.7.3. Murine macrophages J774

Mouse macrophages from the cell line J774 (ATCC TIB-67™) in Dulbecco's Modified Eagle medium (DMEM) supplemented with 10 % heat inactivated fetal bovine serum, penicillin (100 units/mL) and streptomycin (100 µg/mL) at 37°C in a humidified 5 % CO_2 incubator. For the cytotoxicity assay, 12000 cells per well were seeded in a 96 well plate in DMEM medium and were incubated at 37 °C in a 5 % CO_2 atmosphere. Once adhered to the plate, cells were incubated with the indicated compound concentrations for 24 h[30].

2.7.4. Cell viability assays

2.7.4.1. *MTT* viability test

Cell viability was assessed using the MTT (3-(4, 5-dimethylthiazolyl-2)-2, 5-diphenyltetrazolium bromide) assay, where MTT is reduced by metabolically active cells to generate reducing equivalents such as NADH and NADPH, resulting in the formation of an intracellular purple formazan which can be solubilized by the addition of DMSO. Briefly, after time exposition 20 µL of MTT 5 mg/mL were added to each well. Plates

were incubated for 4 h at 37°C in a 5 % CO_2 atmosphere. The medium was removed, the cells were washed 5 times with PBS and the cells were disrupted with 100 µL of DMSO. Plates were kept for 15 min with agitation and absorbance was measured at 570 nm in a Thermo Scientific Varioskan® Flash Multimode plate spectrophotometer[26–31]. Dose-response curves were built and the IC_{50} values were determined using GraphPad Prism version 8.00. The results are presented as averages ± SD (standard deviation) of three independent biological replicates[26–30].

2.7.4.2. Resazurin method

Viability was also tested using resazurin, which is reduced to highly fluorescent resorufin. 50 µL of resazurin solution (2 mg/mL in DMEM) were added to each well and incubated for 4 h at 28 °C or 37 °C. Fluorescence (excitation 530 nm / emission 590 nm) was measured in a Thermo Scientific Varioskan® Flash Multimode plate spectrofluorometer instrument. Dose-response curves were built and the IC_{50} values were determined using GraphPad Prism version 8.00 for Windows. The results are presented as averages ± SD (standard deviation) of three independent biological replicates[26].

3. Results and discussion

3.1 Synthesis and characterization of [Pd(L1)-AuNPs]

The selection of the coordination compound to be conjugated with the AuNPs was made taking into account the previously obtained biological results[7]. Additionally, the chemical structure of this compound made it suitable for use as a linker to prepare the functionalized nanoparticles, as the chloride ligand in the metal coordination sphere is known to be prone to exchange for another ligand like the carboxylate group present in CTPEG12.

The bare AuNPs were prepared according to the described procedure (section 3.2). The amount of the Raman reporter, MGITC, was tuned, testing the effect of different concentrations of MGITC on the properties of the obtained MGITC-AuNP nanotags. In fact, a final concentration of more than 100 nM of MGITC induced remarkable

aggregation of the nanotags, indicated by the broadening and dampening of the characteristic plasmon band at around 520 nm and the appearance of a peak >700 nm due to the formation of larger clusters (Figure S1). This over-aggregation also resulted in a reduction of the SERS signal obtained from the nanotags (Figure S2). An optimum concentration of 40 nM MGITC was selected as this resulted in stable nanotags, which still yielded a strong SERS signal (Figures S3-S4). Further information regarding the size and zeta potential of the obtained nanoparticles is reported in Table S1 and Table S2.

The conjugation of the nanotags with different linkers was assayed and CTPEG12 was selected. CTPEG12 is known for its ability to bind to the surface of AuNPs through the thiol group (SH). Furthermore, the carboxylic acid group on the other side of the CTPEG12 chain would be the site for **[PdCl(L1)]** to bind. In this sense, we have included borate buffer (pH 8.5) in order to leave the carboxylate group in its deprotonated form (COO^-) to favour metal coordination.

Due to solubility issues, the conjugation to the **[PdCl(L1)]** complex was studied performing fixed volume additions of a concentrated stock solution in DMF (1.25 mg/mL). The obtained **[Pd(L1)-AuNPs]** UV-Vis spectra are presented in Figure S5. The observed band for **MGITC-AuNPs** was mainly conserved upon binding to the coordination compound, with a slight redshift from 528 nm in bare nanoparticles to 533 nm, as expected upon conjugation. Volumes of the stock solution ranging from 10 to 80 µL were used and to this extent, nanoparticle aggregation was not observed. In addition, DLS and zeta potential measurements were performed for the different assayed conditions (Tables S3 and S4). The conjugation with **CTPEG12** and **[PdCl(L1)]** leads to an increase of 10-14 nm in the particle size. The SERS signal was also conserved for every batch of **[Pd(L1)-AuNPs]** obtained (Figure 3), however, it is worth noting that an increased background signal was observed for the experiments with the **[PdCl(L1)]** addition, even after washing the samples. This was associated with the presence of the Pd complex on the surface of the nanoparticles, as the compound is fluorescent when excited with the laser in Raman experiments (Figure S6). This provided further evidence that the molecule was successfully attached to the surface of the nanoparticles. The initial intention was to monitor the SERS signal of the **[PdCl(L1)]** directly; however, since a strong fluorescent background was obtained from the complex during Raman

experiments, a Raman reporter (MGITC) had to be incorporated into the nanoparticle conjugates to allow them to be monitored using SERS.

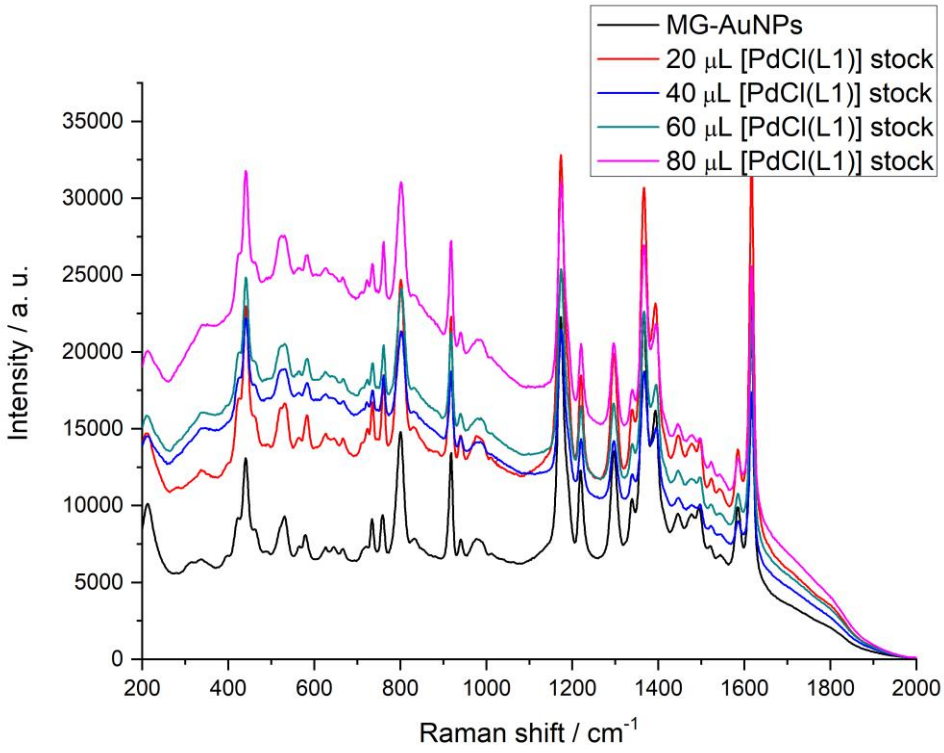

Figure 3. SERS spectrum obtained using a 638 cm^{-1} laser, with 100 % of power and an integration time of 0.1 seconds of **[Pd(L1)-AuNPs]** using different complex concentrations.

Scanning electron microscopy (SEM) allowed us to study the shape and size of the obtained nanoparticles at each stage of the synthetic process. Discrete, spherical shaped nanoparticles were found in every sample measured. Using the software ImageJ®, the diameters of at least one hundred discrete nanoparticles for each batch were measured. The mean size of the obtained nanoparticles increased from approximately 56 nm (56 ± 12 nm) in the bare AuNPs to 70 nm (70 ± 12 nm) in **[Pd(L1)-AuNPs]**. Figure 4 shows selected SEM images and size histograms of the scanned populations.

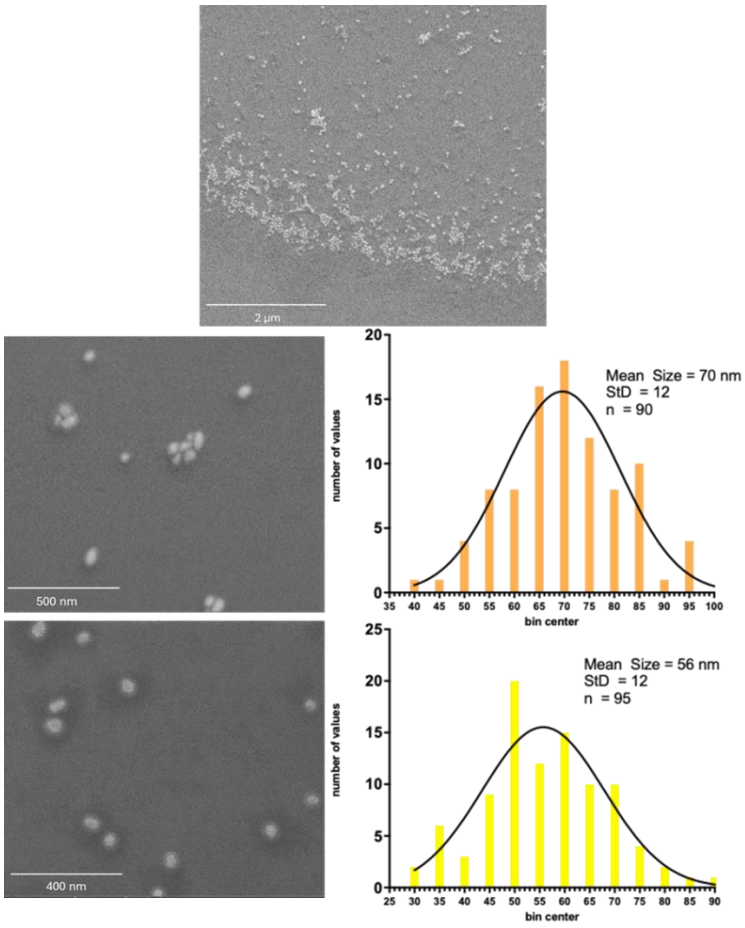

Figure 4. SEM image of obtained bare **AuNPs** and **[Pd(L1)-AuNPs]**. Top: an image of **[Pd(L1)-AuNPs]** obtained nanoparticles using a scale of 2 µm. Middle: a zoomed image (scale of 500 nm) of obtained bare nanoparticles and the corresponding size histogram. Bottom: a zoomed image of **[Pd(L1)-AuNPs]** nanoparticles and the corresponding size histogram. See Figure S7 for details.

ICP-MS studies allowed us to calculate the amount of Pd present in the average gold nanoparticle conjugates. For this, Au and Pd concentrations were determined simultaneously. Then, considering the proposed model (on section 3.5), the amount of Au/nanoparticle was determined and the Pd atoms/AuNP ratio was calculated (Figure 5). The obtained results are comparable to the previously reported values for the conjugation of cisplatin[14]. Additionally, the Pd load and Pd concentration were used in further

experiments in order to adjust the concentration of the **[Pd(L1)-R]** unit in the biological studies.

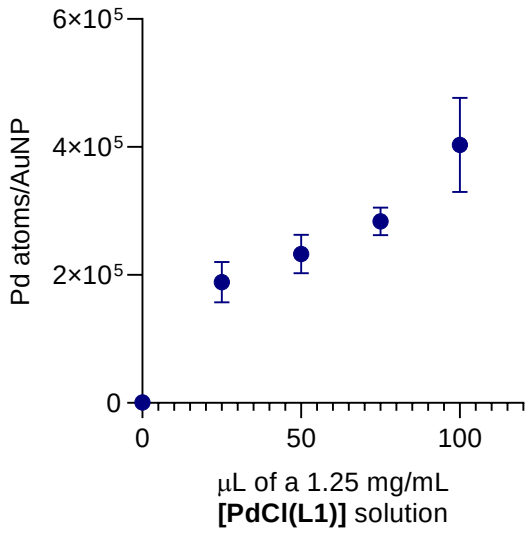

Figure 5. ICP-MS results obtained for **[Pd(L1)-AuNPs]**.

3.2. Biological studies: Trypanosoma brucei brucei

Firstly, a screening assay for anti-trypanosomal activity of the nanoparticles, complex components and conjugated and non-conjugated complex was performed at a standard concentration of 25 µM against *T. b. brucei* bloodstream form parasites (AnTat1.1 strain). All compounds were incubated with the parasites for 24 hours and cell counts compared to control wells containing *T. b. brucei* only (Figure 6). The unconjugated nanoparticles (**MGITC-AuNPs** and bare **AuNPs**) did not affect parasite viability. However, the complex components incubated in isolation with the parasites both showed significant effects on *T. b. brucei*. The palladium salt (**$Na_2[PdCl_4]$**) showed a 47.1 % reduction in cell counts while the free ligand (**HL1)** resulted in a decrease of 56.3 % in the 25 µM dose (calculated as final concentration of Pd using the ICP-MS data). This is in contrast to previous experiments with *T. cruzi* trypomastigotes where no anti-*T. cruzi* activity was observed with HL1[7]. The unconjugated **[PdCl(L1)]** complex caused an even greater decrease in cell viability (91.1%), indicating that the anti-*T. b. brucei* activity of HL1 was

improved upon coordination to Pd (a similar result to what we observed for *T. cruzi*). Finally, the [PdCl(L1)]-conjugated nanoparticles **[Pd(L1)-AuNPs]** demonstrated the greatest anti-*T. b. brucei* activity at 25 µM with a 94.2% reduction in viable cell counts.

.

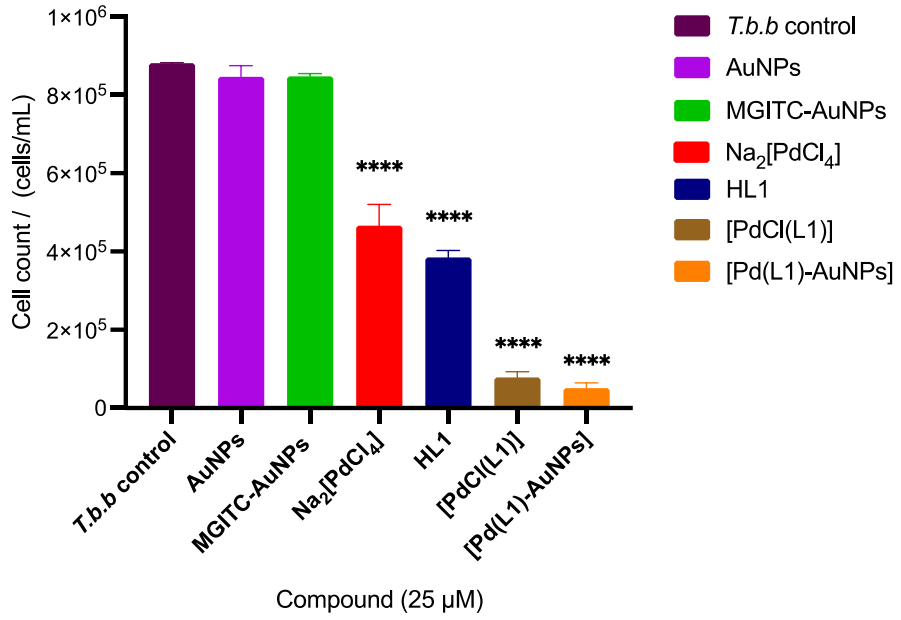

Figure 6. Anti-trypanosomal activities of compounds screened at a fixed dose of 25 µM against *T. b. brucei*, strain Antat1.1. Cell counts/mL after 24 hours incubation are given as Mean and standard deviation, N=3. Compounds which produced a significant reduction in cell counts are indicated by **** (P<0.0001).

Dose response experiments were performed for the free ligand (**HL1**), the **[PdCl(L1)]** complex and the conjugated nanoparticles (**[Pd(L1)-AuNPs]**). In this stage, a **CTPEG12-AuNPs** control was additionally included in order to test if the toxicity effect of the conjugates could be explained by the inclusion of the CTPEG12 linker. As expected, results (Table 1 and Figure S8) showed an increase of the activity from the free **HL1** ligand to **[PdCl(L1)]**. The control **CTPEG12-AuNPs**, presented remarkable activity but the conjugate **[Pd(L1)-AuNPs]** presented the lowest IC_{50} as the result of an increased effect due to both **CTPEG12-AuNPs** and **[PdCl(L1)]**.

Obtained results were in the same order of those reported for the reference drug Nifurtimox in similar experimental conditions (EC_{50} = 15.0 ± 2.5 µM, 427 strain) [32]. The increased activity of the conjugated **[Pd(L1)-AuNPs]** could be related to the ability of **AuNPs** to function as drug carriers. In this sense, **AuNPs** could be responsible for accelerating or enhancing the internalization of the active **[PdCl(L1)]** compound leading to an enhanced antiparasitic effect. Once inside the parasite, both the **AuNPs** and **[PdCl(L1)]** could exert their action both conjugated or independently by acting on different targets.

Table 1. IC_{50} vs *T.b.b.* of the tested compounds

Compound	**HL1**	**[PdCl(L1)]**	**CTPEG12-AuNPs**	**[Pd(L1)-AuNPs]**
IC_{50} *T.b.b.*/ µM (95% CI)	28.37 (25.13-32.97)	15.32 (13.84-17.03)	6.15 (5.26-7.35)	3.22 (2.85-3.68)

3.3. Imaging experiments

The inclusion of the Raman reporter to these conjugated nanoparticles allowed us to explore the *in vitro* imaging of fixed parasites. The Raman spectra of the parasite were obtained using a 532 nm laser (Figure 7, bottom left) and false color images were generated based on the intensity of the selected Raman bands at 2934 cm^{-1} and 3057 cm^{-1} (Figure 7, 1-3), which are associated in literature with the CH_2 asymmetric stretch of constitutive lipids and proteins of the parasite and C-H stretch of lipids present in the of the parasite, respectively[33]. The nanotags were detected using the 633 nm laser (Figure 7, bottom right), where the spectrum shows the characteristic bands of the MGITC containing nanotags (1611 cm^{-1} and 1175 cm^{-1})[34]. Taking into account the high intensities of these bands due to the SERS effect, the background fluorescence of **[Pd(L1)-AuNPs]** conjugates was negligible. Figure 7 (4-6) shows the imaging of a single parasite in different conditions. Using those maps overlapped we observed the presence of the nanotags inside the parasite cells. Furthermore, the nanoparticles appear to be

concentrated in the kinetoplast and the nuclear regions of the parasite, indicated by a maximum intensity of the 1175 cm^{-1} band in these regions (red spots in Figure 7, 6). This result is interesting since those regions (nuclei and kinetoplast) are DNA rich regions[35], which may indicate that the nanoparticles could be targeting this specific biomolecule, maybe thanks to the presence of the Pd atom in the conjugates. Further experiments will be carried out in future research to confirm this hypothesis considering that the stability of **[Pd(L1)-AuNPs]** in the intraparasitic environment could not be assured.

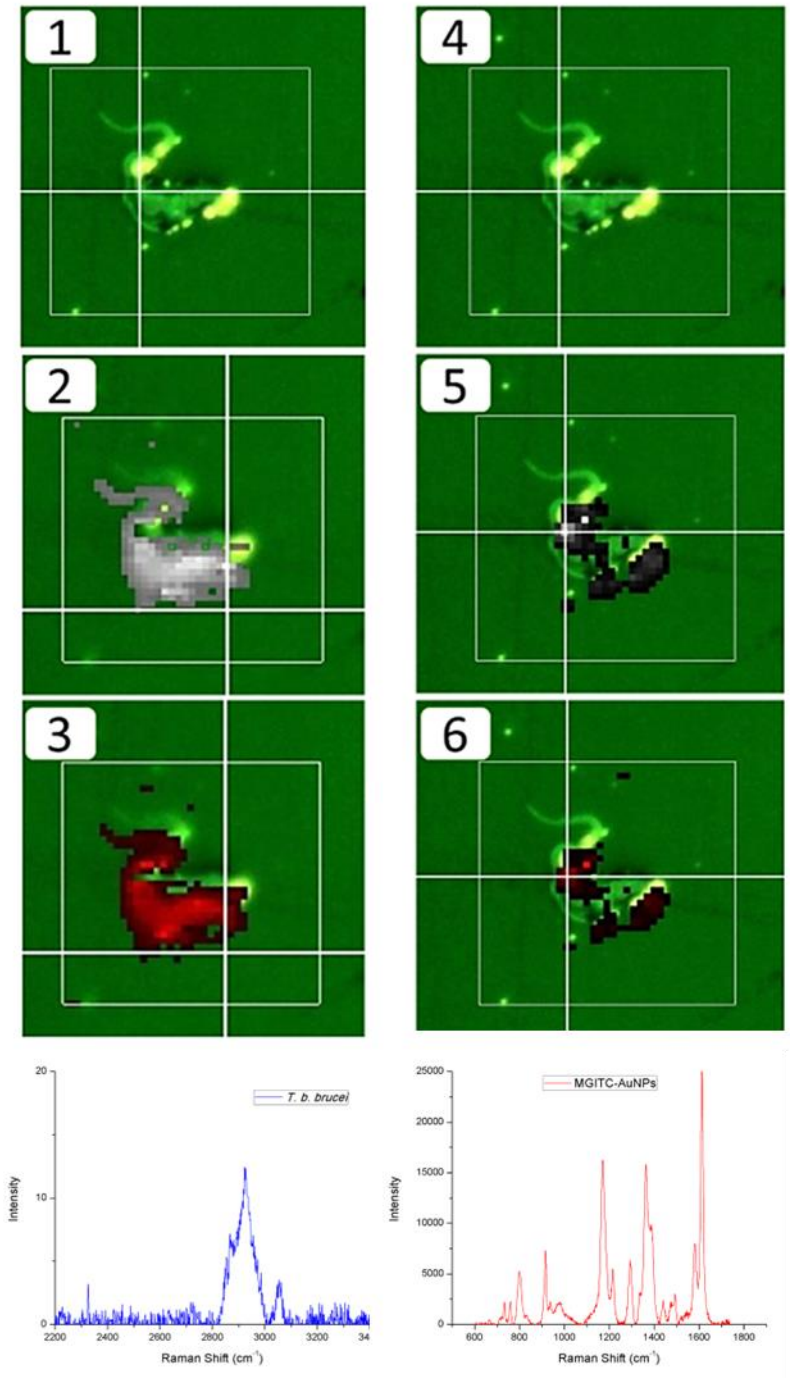

Figure 7. Raman imaging of a single *T. b. b.* cell treated with **[Pd(L1)-AuNPs]**. The images on the left (excitation = 532 cm^{-1}) show (1) a white light image of the parasite cell, (2) false color image based on the intensity of the 2934 cm^{-1} band and (3) false color image based on the intensity of the 3057 cm^{-1} band, each overlaid with the white light image. The bottom left Raman spectrum is a representative spectrum from the *T.b.b.* collected using 532 nm laser excitation. The images on the right (excitation =

633 cm^{-1}) show (4) a white light image of the parasite, (5) intensity of the 1611 cm^{-1} band and (6) intensity of the 1175 cm^{-1} band. The bottom right Raman spectrum is a representative spectrum from the MG-ITC containing nanotags collected using a 633 nm laser excitation.

3.4. Mammalian cells experiments

The cytotoxicity assessments were performed on VERO cells and murine macrophages J774 as mammalian cell models for both **[PdCl(L1)]** and the conjugated gold nanoparticles (**[Pd(L1)-AuNPs]**) (Figures S9 and S10).

Initially, the MTT assay was employed to evaluate cytotoxicity in macrophages. However, determining the IC_{50} values for AuNPs in general proved challenging due to interference with the readout measurements at 570 nm. To eliminate the interference from AuNPs, the cells were washed five times with PBS before the addition of DMSO, but the cells detached easily, preventing absorbance measurements. Consequently, an alternative method, the resazurin reduction assay, was utilized to assess cell viability through fluorescence. Two independent experiments were carried out, each comprising three biological replicates. It was observed that **[Pd(L1)-AuNPs]** exhibited some toxicity for this cell type. No observable effect of **MGITC-AuNPs** was noted at concentrations up to 50 µM. As an alternative approach, toxicity was evaluated in VERO cells using the MTT assay as this cell line is more robust. Results demonstrated that **[Pd(L1)-AuNPs]** were also quite toxic, consistent with the outcomes observed in the macrophage cell line (Table 2 and Table S5).

Table 2. IC_{50} vs J774 macrophages and VERO cells of the tested compounds

Compound	**IC_{50} (µM)* J774 macrophages**	**IC_{50} (µM) VERO cells**
[PdCl(L1)]	6.13 ± 0.51	7.98 ± 0.50
[PdCl(L1)-AuNPs]	1.59 ± 0.09	2.20 ± 0.14

MGITC-AuNPs	>50	>50

*determined using Resazurin assay

However, it should be noted that even though the **[PdCl(L1)]** compound resulted in toxic effects both for J744 macrophages and VERO cells in the experiments showed herein, it had been previously tested in a lactate dehydrogenase (LDH) liberation assay with fresh peritoneal mice macrophages showing no toxicity up to 50 µM. Additionally, the palladium complex participated in an *in vivo* 30 days challenge and all mice survived the complete experiment[7]. Therefore, these specific cellular toxicity results obtained did not prevent **[Pd(L1)-AuNPs]** remaining as good candidates for further *in vivo* studies.

4. Concluding remarks

In this work, we successfully prepared gold nanotags containing the MGITC Raman reporter. Furthermore, the conjugation of the previously reported biologically active complex, **[PdCl(L1)]**, to the nanotags, was achieved. The conjugated nanotags were characterized and tested *in vitro* as anti-*T. brucei brucei* compounds. Results show that, as observed for *T. cruzi*, the complexation of **HL1** to Pd improves the anti-*T.b.b.* activity. Furthermore, the results show that the non-conjugated nanotags (**MGITC-AuNPs**) have anti-*T. b. b.* activity *per se*. Interestingly, the conjugated nanotags **[Pd(L1)-AuNPs]** presented an increase of the anti-*T.b.b.* activity as a result of the combined activity between unconjugated nanotags (**MGITC-AuNPs**) and **[PdCl(L1)]**. Preliminary imaging using Raman microscopy and SERS experiments allowed us to observe the presence of nanoparticles inside the parasites indicating good uptake. In this sense, to get insight in the intraparasitic distribution of the obtained nanotags, further studies are necessary including other Raman reporters that could avoid potential background noise from the cell's components. The *in vitro* selectivity of **[PdCl(L1)]** was not improved as a consequence of conjugation with **AuNPs** and the cytotoxicity of the conjugates could be a challenge for the proposed applications. However, based on our previously reported

results for **[PdCl(L1)]**, *in vitro* cellular toxicity does not necessarily parallel animal toxicity, so it is still worthwhile to test the performance of the obtained conjugates *in vivo*. This study successfully demonstrated the improvement in drug activity by conjugation to gold nanoparticles, and the ability to track the location of the resulting conjugates in cells, indicating the potential of drug-nanoparticle conjugates for future *in vivo* studies as antiparasitic agents.

Conflicts of interest: There are no conflicts to declare.

Data availability: Most data supporting this article have been included as part of the Supporting Information.

Supporting Information: UV-Vis spectra of MGITC-AuNPs prepared with different concentrations of MGITC. Range from 0 to 1000 nM, Raman spectra (638 nm laser, 100 % laser power, 1s accumulation time) of MGITC-AuNPs prepared with different concentrations of MGITC, UV-Vis spectra of MGITC-AuNPs prepared with different concentrations of MGITC, Raman spectra (638 nm laser, 100 % laser power, 1s accumulation time) of MGITC-AuNPs prepared with different concentrations of MGITC, DLS measurements of MGITC-AuNPs prepared with different concentrations of MGITC, Zeta potential of MGITC-AuNPs prepared with different concentrations of MGITC, DLS measurements of [Pd(L1)-AuNPs] prepared with different concentrations of [PdCl(L1)] stock solution, Zeta potential of [Pd(L1)-AuNPs] prepared with different concentrations of [PdCl(L1)] stock solution, UV-Vis spectra of [Pd(L1)-AuNPs] prepared with different concentrations of [PdCl(L1)], Raman spectra (633 nm laser, 1 % laser power, 10 s accumulation time) of [PdClL1] measured in solid state, SEM images obtained for A) Bare AuNPs, B) [Pd(L1)-AuNPs] and the corresponding size histograms, Dose-response plots for compounds and conjugates versus *T. b. b*., Dose-response curve of [PdCl(L1)] compound against macrophages J774.

Acknowledgements: SR thanks Agencia Nacional de Investigación e Innovación (ANII) for the PhD grant number POS_NAC_D_2020_1_164085 and CAP-UdelaR for the PhD grant. LO, GM, LP and GS thank Programa de Desarrollo de las Ciencias Básicas

(PEDECIBA). S.L. and D.G. acknowledge funding from Engineering and Physical Sciences Research Council (EPSRC) through grant number EP/X037770/1.

References

(1) Gambino, D.; Otero, L. Facing Diseases Caused by Trypanosomatid Parasites: Rational Design of Pd and Pt Complexes With Bioactive Ligands. *Front. Chem.* **2022**, *9*, 816266. https://doi.org/10.3389/fchem.2021.816266.

(2) Franz, K. J.; Metzler-Nolte, N. Introduction: Metals in Medicine. *Chem. Rev.* **2019**, *119* (2), 727–729.

(3) Otero, L.; Vieites, M.; Boiani, L.; Denicola, A.; Rigol, C.; Opazo, L.; Olea-Azar, C.; Maya, J. D.; Morello, A.; Krauth-Siegel, R. L.; Piro, O. E.; Castellano, E.; González, M.; Gambino, D.; Cerecetto, H. Novel Antitrypanosomal Agents Based on Palladium Nitrofurylthiosemicarbazone Complexes: DNA and Redox Metabolism as Potential Therapeutic Targets †. *J. Med. Chem.* **2006**, *49* (11), 3322–3331. https://doi.org/10.1021/jm0512241.

(4) Cipriani, M.; Toloza, J.; Bradford, L.; Putzu, E.; Vieites, M.; Curbelo, E.; Tomaz, A. I.; Garat, B.; Guerrero, J.; Gancheff, J. S.; Maya, J. D.; Olea Azar, C.; Gambino, D.; Otero, L. Effect of the Metal Ion on the Anti *T. Cruzi* Activity and Mechanism of Action of 5-Nitrofuryl-Containing Thiosemicarbazone Metal Complexes. *Eur. J. Inorg. Chem.* **2014**, *2014* (27), 4677–4689. https://doi.org/10.1002/ejic.201402614.

(5) World Health Organization (WHO). *Chagas disease (also known as American trypanosomiasis)*. https://www.who.int/news-room/fact-sheets/detail/chagas-disease-(american-trypanosomiasis).

(6) Fall, F.; Mamede, L.; Schioppa, L.; Ledoux, A.; De Tullio, P.; Michels, P.; Frédérich, M.; Quetin-Leclercq, J. Trypanosoma Brucei: Metabolomics for Analysis of Cellular Metabolism and Drug Discovery. *Metabolomics* **2022**, *18* (4), 20.

(7) Rostán, S.; Porto, S.; Barbosa, C. L. N.; Assis, D.; Alvarez, N.; Machado, F. S.; Mahler, G.; Otero, L. A Novel Palladium Complex with a Coumarin-Thiosemicarbazone Hybrid Ligand Inhibits Trypanosoma Cruzi Release from Host Cells and Lowers the Parasitemia in Vivo. *JBIC J. Biol. Inorg. Chem.* **2023**. https://doi.org/10.1007/s00775-023-02020-2.

(8) H. Lopes, A. Trypanosomatids: Odd Organisms, Devastating Diseases. *Open Parasitol. J.* **2010**, *4* (1), 30–59. https://doi.org/10.2174/1874421401004010030.

(9) Simarro, P.; Franco, J.; Diarra, A.; Jannin, J. Epidemiology of Human African Trypanosomiasis. *Clin. Epidemiol.* **2014**, 257. https://doi.org/10.2147/CLEP.S39728.

(10) World Health Organization. *Trypanosomiasis, human African (sleeping sickness)*. Trypanosomiasis, human African (sleeping sickness). Trypanosomiasis, human African (sleeping sickness).

(11) Parreira De Aquino, G.; Mendes Gomes, M. A.; Köpke Salinas, R.; Laranjeira-Silva, M. F. Lipid and Fatty Acid Metabolism in Trypanosomatids. *Microb. Cell* **2021**, *8* (11), 262–275. https://doi.org/10.15698/mic2021.11.764.

(12) Hofer, A. Targeting the Nucleotide Metabolism of *Trypanosoma Brucei* and Other Trypanosomatids. *FEMS Microbiol. Rev.* **2023**, *47* (3), fuad020. https://doi.org/10.1093/femsre/fuad020.

(13) Patil, T.; Gambhir, R.; Vibhute, A.; Tiwari, A. P. Gold Nanoparticles: Synthesis Methods, Functionalization and Biological Applications. *J. Clust. Sci.* **2023**, *34* (2), 705–725. https://doi.org/10.1007/s10876-022-02287-6.

(14) Craig, G. E.; Brown, S. D.; Lamprou, D. A.; Graham, D.; Wheate, N. J. Cisplatin-Tethered Gold Nanoparticles That Exhibit Enhanced Reproducibility, Drug Loading, and Stability: A Step Closer to Pharmaceutical Approval? *Inorg. Chem.* **2012**, *51* (6), 3490–3497.

(15) Brown, S. D.; Nativo, P.; Smith, J.-A.; Stirling, D.; Edwards, P. R.; Venugopal, B.; Flint, D. J.; Plumb, J. A.; Graham, D.; Wheate, N. J. Gold Nanoparticles for the Improved Anticancer Drug Delivery of the Active Component of Oxaliplatin. *J. Am. Chem. Soc.* **2010**, *132* (13), 4678–4684. https://doi.org/10.1021/ja908117a.

(16) Choudhury, S. D. Nano-Medicines a Hope for Chagas Disease! *Front. Mol. Biosci.* **2021**, *8*, 655435. https://doi.org/10.3389/fmolb.2021.655435.

(17) Benelli, G. Gold Nanoparticles – against Parasites and Insect Vectors. *Acta Trop.* **2018**, *178*, 73–80. https://doi.org/10.1016/j.actatropica.2017.10.021.

(18) Adeyemi, O. S.; Molefe, N. I.; Awakan, O. J.; Nwonuma, C. O.; Alejolowo, O. O.; Olaolu, T.; Maimako, R. F.; Suganuma, K.; Han, Y.; Kato, K. Metal Nanoparticles Restrict the Growth of Protozoan Parasites. *Artif. Cells Nanomedicine Biotechnol.* **2018**, *46* (sup3), 86–94. https://doi.org/10.1080/21691401.2018.1489267.

(19) Adeyemi, O. S.; Whiteley, C. G. Interaction of Nanoparticles with Arginine Kinase from Trypanosoma Brucei: Kinetic and Mechanistic Evaluation. *Int. J. Biol. Macromol.* **2013**, *62*, 450–456. https://doi.org/10.1016/j.ijbiomac.2013.09.008.

(20) Bajwa, H. U. R.; Khan, M. K.; Abbas, Z.; Riaz, R.; Rehman, T. U.; Abbas, R. Z.; Aleem, M. T.; Abbas, A.; Almutairi, M. M.; Alshammari, F. A.; Alraey, Y.; Alouffi, A. Nanoparticles: Synthesis and Their Role as Potential Drug Candidates for the Treatment of Parasitic Diseases. *Life* **2022**, *12* (5), 750. https://doi.org/10.3390/life12050750.

(21) Yang, J.; Wang, Z.; Zong, S.; Chen, H.; Zhang, R.; Cui, Y. Dual-Mode Tracking

of Tumor-Cell-Specific Drug Delivery Using Fluorescence and Label-Free SERS Techniques. *Biosens. Bioelectron.* **2014**, *51*, 82–89. https://doi.org/10.1016/j.bios.2013.07.034.

(22) Mei, R.; Wang, Y.; Zhao, X.; Kang, Q.; Shen, D.; Chen, L. Near-Infrared Light-Responsive SERS Tags Enable Positioning and Monitoring of the Drug Release of Photothermal Nanomedicines In Vivo. *Anal. Chem.* **2021**, *93* (49), 16590–16597. https://doi.org/10.1021/acs.analchem.1c03949.

(23) Fei, J.; Wu, L.; Zhang, Y.; Zong, S.; Wang, Z.; Cui, Y. Pharmacokinetics-on-a-Chip Using Label-Free SERS Technique for Programmable Dual-Drug Analysis. *ACS Sens.* **2017**, *2* (6), 773–780. https://doi.org/10.1021/acssensors.7b00122.

(24) Turkevich, J.; Stevenson, P. C.; Hillier, J. A Study of the Nucleation and Growth Processes in the Synthesis of Colloidal Gold. *Discuss. Faraday Soc.* **1951**, *11*, 55–75.

(25) Rahman, A.; Rahman, A.; Ghann, W.; Kang, H. G.; Uddin, J. Terahertz Multispectral Imaging for the Analysis of Gold Nanoparticles' Size and the Number of Unit Cells in Comparison with Other Techniques. *Int J Biosens Bioelectron* **2018**, *4*, 159–164.

(26) Scalese, G.; Machado, I.; Salinas, G.; Pérez-Díaz, L.; Gambino, D. Heteroleptic Oxidovanadium (V) Complexes with Activity against Infective and Non-Infective Stages of Trypanosoma Cruzi. *Molecules* **2021**, *26* (17), 5375.

(27) Scalese, G.; Machado, I.; Correia, I.; Pessoa, J. C.; Bilbao, L.; Pérez-Diaz, L.; Gambino, D. Exploring Oxidovanadium (Iv) Homoleptic Complexes with 8-Hydroxyquinoline Derivatives as Prospective Antitrypanosomal Agents. *New J. Chem.* **2019**, *43* (45), 17756–17773.

(28) Scalese, G.; Machado, I.; Fontana, C.; Risi, G.; Salinas, G.; Pérez-Díaz, L.; Gambino, D. New Heteroleptic Oxidovanadium (V) Complexes: Synthesis, Characterization and Biological Evaluation as Potential Agents against Trypanosoma Cruzi. *JBIC J. Biol. Inorg. Chem.* **2018**, *23*, 1265–1281.

(29) Soba, M.; Scalese, G.; Casuriaga, F.; Pérez, N.; Veiga, N.; Echeverría, G. A.; Piro, O. E.; Faccio, R.; Pérez-Díaz, L.; Gasser, G. Multifunctional Organometallic Compounds for the Treatment of Chagas Disease: Re (i) Tricarbonyl Compounds with Two Different Bioactive Ligands. *Dalton Trans.* **2023**, *52* (6), 1623–1641.

(30) Rivas, F.; Del Mármol, C.; Scalese, G.; Pérez-Díaz, L.; Machado, I.; Blacque, O.; Medeiros, A.; Comini, M.; Gambino, D. New Multifunctional Ru (II) Organometallic Compounds Show Activity against Trypanosoma Brucei and Leishmania Infantum. *J. Inorg. Biochem.* **2022**, *237*, 112016.

(31) Scalese, G.; Correia, I.; Benítez, J.; Rostán, S.; Marques, F.; Mendes, F.; Matos, A. P.; Pessoa, J. C.; Gambino, D. Evaluation of Cellular Uptake, Cytotoxicity and

Cellular Ultrastructural Effects of Heteroleptic Oxidovanadium (IV) Complexes of Salicylaldimines and Polypyridyl Ligands. *J. Inorg. Biochem.* **2017**, *166*, 162–172.

(32) Franco, J.; Medeiros, A.; Benítez, D.; Perelmuter, K.; Serra, G.; Comini, M. A.; Scarone, L. In Vitro Activity and Mode of Action of Distamycin Analogues against African Trypanosomes. *Eur. J. Med. Chem.* **2017**, *126*, 776–788. https://doi.org/10.1016/j.ejmech.2016.12.002.

(33) Girard, A.; Cooper, A.; Mabbott, S.; Bradley, B.; Asiala, S.; Jamieson, L.; Clucas, C.; Capewell, P.; Marchesi, F.; Gibbins, M. P.; Hentzschel, F.; Marti, M.; Quintana, J. F.; Garside, P.; Faulds, K.; MacLeod, A.; Graham, D. Raman Spectroscopic Analysis of Skin as a Diagnostic Tool for Human African Trypanosomiasis. *PLOS Pathog.* **2021**, *17* (11), e1010060. https://doi.org/10.1371/journal.ppat.1010060.

(34) Verdin, A.; Sloan-Dennison, S.; Malherbe, C.; Graham, D.; Eppe, G. SERS Nanotags for Folate Receptor α Detection at the Single Cell Level: Discrimination of Overexpressing Cells and Potential for Live Cell Applications. *The Analyst* **2022**, *147* (14), 3328–3339. https://doi.org/10.1039/D2AN00706A.

(35) Woodward, R.; Gull, K. Timing of Nuclear and Kinetoplast DNA Replication and Early Morphological Events in the Cell Cycle of *Trypanosoma Brucei*. *J. Cell Sci.* **1990**, *95* (1), 49–57. https://doi.org/10.1242/jcs.95.1.49.

This is the accepted manuscript of: Rostán, S., Laing, S., Girard, A., Scalese, G., Cooper, A., MacLeod, A., Pérez-Díaz, L., Mahler, G., Faulds, K., Graham, D., & Otero, L. (2024). Gold nanoparticle-based conjugated nanotags as potential compounds against Trypanosoma brucei infection. *ACS Applied Nano Materials*, *7*(24), 28219-28228. https://doi.org/10.1021/acsanm.4c05201.

TOC